ROYAL SOCIETY OPEN SCIENCE

royalsocietypublishing.org/rsos

Research

Cite this article: Plank MJ, Young AR, Senior KL, Tobin RJ, O'Hara-Wild M, Callaghan F, Shearer FM, Eales O. 2026 Multi-pathogen situational assessment and forecasting of respiratory disease in Aotearoa New Zealand. *R. Soc. Open Sci.* **13**: 260536.
https://doi.org/10.1098/rsos.260536

Received: 13 March 2026
Accepted: 25 June 2026

Subject Category:
Mathematics

Subject Areas:
health and disease, epidemiology, biomathematics, mathematical modelling

Keywords:
Bayesian P-splines, disease surveillance, hidden-state model, infectious disease epidemiology, public health, mathematical modelling

Author for correspondence:
Michael J. Plank
e-mail: michael.plank@canterbury.ac.nz

Supplementary material is available online at https://doi.org/10.6084/m9.figshare.c.8598184.

THE ROYAL SOCIETY PUBLISHING

Multi-pathogen situational assessment and forecasting of respiratory disease in Aotearoa New Zealand

Michael J. Plank[1], Alys R. Young[2,4], Katharine L. Senior[2,5], Ruarai J. Tobin[2,3], Mitchell O'Hara-Wild[6], Fiona Callaghan[7], Freya M. Shearer[2,5] and Oliver Eales[2,3]

[1]School of Mathematics and Statistics, University of Canterbury, Christchurch, New Zealand
[2]School of Population and Global Health and [3]School of Mathematics and Statistics, University of Melbourne, Melbourne, Victoria, Australia
[4]College of Science and Engineering, James Cook University, Townsville, Queensland, Australia
[5]Infectious Disease Ecology and Modelling Team, The Kids Research Institute Australia, Western Australia, Australia
[6] Monash University, Melbourne, Victoria, Australia
[7]Public Health Agency, Manatū Hauora Ministry of Health, Wellington, New Zealand

MJP, 0000-0002-7539-3465; RT, 0000-0002-5202-240X; FMS, 0000-0001-9600-3473; OE, 0000-0002-8086-4495

Real-time analysis of epidemic trends and forecasts can help support public health planning and the response to seasonal respiratory disease. Here, we present two models that were used in a 2025 New Zealand winter situational assessment programme for three respiratory pathogens: SARS-CoV-2, influenza and respiratory syncytial virus (RSV). Data on SARS-CoV-2 were obtained from the national Covid-19 surveillance system; data on influenza and RSV were limited to a sentinel hospital surveillance programme. Models were run weekly from May to October 2025 on these real-time disease surveillance data and provided a quantitative representation of the current epidemic trend, along with estimates of the epidemic growth rate and 28-day ahead forecasts of case incidence. Model results and interpretation were provided in weekly reports to public health partners as part of a trans-Tasman winter programme run by the Australia–Aotearoa Consortium for Epidemic Forecasting and Analytics (ACEFA). We compare in-season results that were included in these reports to a retrospective analysis of the complete data for the season. We conclude that real-time analyses performed reasonably well and identify some areas for improvement in future winter situational assessment programmes.

1. Introduction

Analysis of current epidemic trends and near-term forecasts can contribute to situational awareness and support healthcare capacity planning [1,2]. This is particularly relevant during the winter respiratory illness season, when healthcare capacity is often stretched [3] due to overlapping respiratory pathogen epidemics. Real-time analysis and forecasting models can help anticipate and plan for increases in hospitalizations or patient load.

Aggregate metrics, such as severe acute respiratory illness, or syndromic surveillance indicators such as influenza-like illness, are routinely used to monitor the progression of the respiratory illness season. However, these aggregate metrics can mask trends in the composite pathogens that contribute to the aggregate metric [4]. For example, a decreasing trend in an aggregate metric could mask a growing epidemic of a singe-component pathogen and, therefore, lead to underestimation of future healthcare demand. Quantifying pathogen-specific trends (or strain-specific trends where relevant) provides richer and more valuable information than assessing trends in aggregate metrics alone [5].

Real-time trend analysis and forecasts have been applied to a variety of pathogens including influenza [6,7], dengue [8], Zika [9], Ebola [10] and diphtheria [11]. They can also play an important role in pandemic response by adding an early warning dimension to pandemic respiratory surveillance and were used extensively during the COVID-19 pandemic [12–15].

In this paper, we describe a winter situational assessment programme for respiratory diseases, which was implemented for the first time in New Zealand in 2025. This programme was run by the Australia–Aotearoa Consortium for Epidemic Forecasting and Analytics (ACEFA) that oversees a trans-Tasman situational assessment programme, including the Australia–Aotearoa Forecasting Hub [16]. This hub reflects the structure and activities of other infectious disease forecasting hubs around the world [8].

Our analysis focuses on two important components of situational assessment: real-time epidemic trend analysis and short-term forecasting. We present two separate models, developed by two independent teams, one for trend analysis and one for forecasting. Both of these models were applied to the same surveillance data streams representing SARS-CoV-2, influenza and respiratory syncytial virus (RSV) activity in New Zealand. Our trend analysis model uses Bayesian P-splines [17] to model a case or hospitalization incidence time series as a smooth function of time. This allows us to estimate quantities such as the epidemic growth rate and the effective reproduction number.

Our forecasting model is a latent state model with a renewal process for daily infection incidence [18] and a time-varying reproduction number [19]. The observed variables are daily case notifications and, where available, new daily hospital admissions (each of which is some fraction of infections, observed after a distributed time delay). The model is fitted to data using a particle filter (i.e. sequential Monte Carlo) approach [20].

For both models, we compare in-season results that were used in real time reporting to public health partners against retrospective analysis of complete data for the 2025 season.

2. Methods

2.1. Data

We obtained two de-identified unit record datasets from Te Whatu Ora Health New Zealand. The first dataset contained all polymerase chain reaction (PCR)-confirmed cases of SARS-CoV-2 in New Zealand since 26 February 2020, including admission date for patients admitted to hospital for treatment for COVID-19. This covers the national population of approximately 5.3 million people [21]. During the study period, most PCR testing for SARS-CoV-2 was carried out in hospital settings, and all PCR results and related hospital admissions were reported to the national Public Health Agency and stored in a central data repository. The Public Health Agency categorizes hospital admissions as SARS-CoV-2-related or incidental using two different sources of data. The first data source (the 'inpatient database') is available in near-real-time but includes probable SARS-CoV-2 hospitalizations. The second data source (the 'national minimum dataset') is based on the final clinical coding, which is more reliable but is delayed, as hospital events are only required to be loaded into the dataset within 21 days after the month of discharge [22]. We did not have access to the raw clinical datasets, only the categorization updated in real time by the Public Health Agency. This meant that revisions occurred to real-time counts due to hospital

admissions being retrospectively added to the data, and due to admissions being later re-categorized as not SARS-CoV-2-related. However, the frequency and magnitude of these revisions were not known in advance.

The second dataset contained all patients admitted overnight to one of the four hospitals in the Auckland and Counties Manukau Districts (Kidz First Children's Hospital, Starship Children's Hospital, Middlemore Hospital and Auckland City Hospital) with severe acute respiratory infection (SARI) and who tested positive for either influenza or RSV since 2 January 2025. These data were collected by Public Health and Forensic Science as part of New Zealand's sentinel hospital-based SARI surveillance system [23,24].

Note that the SARS-CoV-2 data are national, while the influenza and RSV data are from a regional sentinel surveillance programme. This covers the largest health region in New Zealand with a population of around 1.2 million people [21] (i.e. around 23% of the national total) with similar socioeconomic and demographic characteristics to the New Zealand population [23]. The different population catchments preclude comparisons of the absolute number of cases between SARS-CoV-2 and either influenza or RSV, although comparisons in epidemic dynamics, such as the timing of the winter peak, are still possible with appropriate caveats. As with many clinical-based respiratory disease surveillance programmes, the data relate to cases presenting to the healthcare system with acute respiratory symptoms. In addition, since the surveillance is primarily hospital-based, cases are further skewed towards the severe end of the clinical spectrum and are not necessarily representative of acute respiratory infections in the wider community.

Weekly updates to each dataset were provided throughout the 2025 winter season (15 rounds). For any given dataset, we refer to the latest date on which data were available as the origin date. The final update was received on 23 October 2025 and contained data up to 10 October 2025. From each update of the unit record data, we calculated the daily total recorded number of laboratory-confirmed: SARS-CoV-2 case notifications, new SARS-CoV-2 hospital admissions, new influenza hospital admissions and new RSV hospital admissions.

2.2. Model for trend analysis

We used a Bayesian P-spline model to quantify the past and current trends in two time series: (i) SARS-CoV-2 case incidence and (ii) SARS-CoV-2, influenza and RSV hospitalization incidence. The model has been described in full elsewhere [5]. In brief, we model the logarithm of the expected value of a time series (i.e. cases and hospitalizations) as a smooth function of time, $s(t)$, using a penalized-spline. A penalized-spline is a linear combination of N basis splines of degree n, $B_{i,n}(t)$:

$$s(t) = \sum_{i}^{N} b_i B_{i,n}(t), \tag{2.1}$$

where b_i are the basis spline coefficients. For any time series, we define a system of third-order basis splines over regularly spaced knots. We set adjacent knots five days apart—this has previously been shown to be a fine enough temporal resolution to capture dynamical effects of SARS-CoV-2 infection prevalence time-series data [25]. The system of basis splines extends three knots on either side of the time series to prevent edge effects. We assume a second-order random-walk prior on the basis spline coefficients:

$$b_i = 2b_{i-1} - b_{i-2} + u_i, \tag{2.2}$$

where

$$u_i \sim N(0, \tau^2). \tag{2.3}$$

This prior penalizes changes in the first derivative of the smoothed function (i.e. changes to the growth rate), with the degree of penalization set by the additional parameter τ. We assume that time-series data, $C(t)$, are negative binomially distributed:

$$C(t) \sim \text{NegBin}(e^{s(t)}, k), \tag{2.4}$$

with an additional parameter k setting the over-dispersion of the data.

We fit the model using a No-U-Turns Sampler [26] implemented in RStan [27]. For all model fits, we confirmed that all parameters had an R-hat less than 1.02 and an effective sample size greater than 400. When fitting the model to the SARS-CoV-2 case and hospitalization time series, we assume uninformative constant prior distributions for the parameters τ and k. When fitting the model to influenza and RSV hospitalization time series, we assume an informative normally distributed prior distribution for both τ and k, with mean and standard deviation taken as the mean and standard deviation of the posterior distributions of the model fit to SARS-CoV-2 hospitalizations (for the same week of reporting). This was done to allow the model to converge when fitting to the shorter influenza and RSV time series. We also performed a sensitivity analysis by fitting the model (to the final dataset) assuming the mean of the informative prior distribution for τ was 0.5 or 2 times the posterior distribution of the model fit to SARS-CoV-2 hospitalizations.

For weekly reporting, the Bayesian P-spline models were fitted to each dataset as received in real time over the course of the season. The Bayesian P-spline model was fitted to the previous three years of data (up to the last day of data available in real time) for SARS-CoV-2 cases and hospitalizations. The model was fitted to the entire continuous time series for influenza and RSV hospitalizations (first day of available continuous data was 2 January 2025, until last day of data available in real time). When fitting the model to SARS-CoV-2 case time series, we additionally account for day-of-the-week effects in the time series (see [5]). As a sensitivity analysis, we also fit the Bayesian P-spline model to the final dataset for SARS-CoV-2 cases, but only including data up to the final day of data received in real time. This was done to evaluate the effect of data revisions on real-time estimates.

2.3. Forecasting model

For the forecasting model, we assume that the time-dependent reproduction number, R_t, follows a zero-mean Gaussian process in log-transformed space:

$$\ln(R_t) \sim GP\left(0, k(t,t')\right). \tag{2.5}$$

We use the Matern 5/2 covariance function defined by

$$k(t,t') = \frac{s_0^2 2^{-3/2}}{\Gamma(5/2)}\left(\frac{\sqrt{2\nu}|t-t'|}{l}\right)^{5/2} K_{5/2}\left(\frac{\sqrt{5}|t-t'|}{l}\right), \tag{2.6}$$

where s_0 is the signal standard deviation, l is the correlation time scale and K_ν is the modified Bessel function of the second kind and order ν. To implement the Gaussian process model, the value of $\ln(R_t)$ is drawn conditional on the known values of $\ln(R_s)$ for $s = 0, \ldots, t-1$ using the method described in [28], with Gaussian observation noise with standard deviation s_n.

We assume the number of new daily infections I_t on day t follows the Poisson renewal process:

$$I_t \sim \text{Poiss}\left(R_t \sum_{s=1}^{m_g} g_s I_{t-s}\right), \tag{2.7}$$

where g_s is the probability mass function for the generation interval ($s = 1, \ldots, m_g$) and m_g is the maximum generation interval.

The expected number of infections with a report date on day t (Z_t) and the expected number of infections with a hospital admission date on day t (H_t) are calculated via forward convolutions:

$$Z_t = \sum_{s=0}^{m_r} u_s I_{t-s}, \tag{2.8}$$

$$H_t = \sum_{s=0}^{m_h} v_s I_{t-s}, \tag{2.9}$$

where u_s and v_s are the probability mass functions of the distribution of time from infection to reporting and time from infection to hospital admission, respectively, and m_r and m_h are their respective maximum values.

We assume that the case–hospitalization ratio P_t on day t follows a Gaussian random walk in log-transformed space with fixed variance σ_P^2:

$$\ln(P_{t+1}) \sim N(\ln(P_t), \sigma_P^2). \tag{2.10}$$

Although this assumption effectively restricts how rapidly the case–hospitalization ratio can change, we found it to be reasonable based on previous data on SARS-CoV-2 cases and hospitalizations for the past 12 months (noting that this excluded periods in which there were major changes in testing programmes, age-dependent contact rates or vaccination rates, which could drive a more rapid change in P_t). We also monitored the estimated value of P_t and associated model fit throughout the season (see §3).

We assume that the observed number of cases, C_t, and new hospital admissions, A_t, on day t are drawn from conditionally independent negative binomial distributions (parametrized by mean and dispersion):

$$C_t \sim \text{NegBin}\left(p_c \omega_{c,t} Z_t, k_c\right), \tag{2.11}$$

$$A_t \sim \text{NegBin}\left(p_c \omega_{h,t} P_t H_t, k_h\right), \tag{2.12}$$

where p_c is the proportion of infections that are reported as cases (assumed to be fixed) and $\omega_{c,t}$ and $\omega_{h,t}$ are day-of-the-week effects for reported cases and hospital admissions, respectively. Note that the latent variables Z_t and H_t include all infections, whereas the observed variables C_t and A_t represent the subset of infections that were reported as cases or hospitalized, respectively. The case ascertainment ratio p_c is non-identifiable from the data, and so we set $p_c = 1$. This means that the latent variable I_t should be interpreted as the daily incidence of new infections that will eventually be reported as cases, as opposed to the actual number of infections, which is unknown. In reality, case ascertainment could vary over time, which could affect forecast performance. However, as surveillance effort over the season is consistent, we believe variations in case ascertainment are likely to be relatively small and to occur slowly relative to the time scale for a seasonal epidemic and the forecasting time horizon of 28 days.

Equations (2.11)–(2.12) define a likelihood function for a given observed value of C_t in terms of $\omega_{c,t} Z_t$ and for a given observed value of A_t in terms of $\omega_{h,t} P_t H_t$. Note that the model includes the flexibility to specify either or both of these distributions as a Poisson distribution by setting the relevant dispersion parameter $k = \infty$.

We estimate the day-of-the-week effects, $\omega_{c,t}$ and $\omega_{h,t}$, directly from the data via

$$\omega_{*,t} = \frac{7 \sum_{s=t \bmod 7} \tilde{X}_s}{\sum_t \tilde{X}_t}, \tag{2.13}$$

where $\tilde{X}_t$ is the relevant observed quantity (either reported cases for $\omega_{c,t}$ or hospital admissions for $\omega_{h,t}$) on day t. The summations are taken over an integer number of weeks leading up to the origin date, up to a maximum of 16 weeks, depending on how much past data are available. This assumes that the day-of-the-week effects are constant over this time period, which may not always be the case. One alternative would be to fit a time-varying day-of-the-week effect model. However, we decided not to do this as it would introduce substantial additional complexity and would risk masking real epidemic trends by subsuming them into fitted day-of-the-week effects. Another alternative would be to ignore day-of-the-week effects completely, or aggregate data to weekly periods. However, this would lose important information and compromise the model's ability to pick up on short-term changes in the epidemic trend.

For details of the initialization and fitting method, see supplementary material, §S1. Parameter values used in the model are listed in table 1. The parameters for the generation interval and delay distributions were estimated from the literature (see supplementary material, §1.3 for details). The parameters of the Gaussian process s_0 and l, and the observation noise parameters k_c and k_h were calibrated manually to achieve a good visual model fit. In principle, these parameters could be inferred from the data with suitable uncertainty. However, we chose not to do this due to the need to balance model complexity with computational limitations for real-time deployment. The parameter P_{CV} is for initialization purposes only and does not affect model fit or forecasts, provided that the model is run for a sufficient time period.

We evaluated probabilistic forecasts y against subsequently observed data y^{obs} using the continuous ranked probability score (CRPS), defined as

$$\text{CRPS}\left(y, y^{\text{obs}}\right) = \int_{-\infty}^{\infty} \left(F(y) - \mathbb{I}\left(y > y^{\text{obs}}\right)\right)^2 dy, \tag{2.14}$$

Table 1. Table of forecasting model parameter values. Parameters shown as $\mu \pm \sigma$ show the mean (μ) and standard deviation (σ) of the assumed distribution. Note that the model nominally assumes $p_c = 1$ (meaning that all modelled infections are eventually reported as cases), but this parameter does not affect model output for observed variables (daily cases and hospital admissions), only for the latent daily infection variable I_t, which we treat as being identifiable only up to multiplication by an unknown case ascertainment ratio, which we assume to be constant.

	SARS-CoV-2	Influenza	RSV
pathogen-specific parameters			
generation interval	3.3 ± 3.5 days	2.6 ± 1.3 days	7.5 ± 2.1 days
time from infection to reporting	6.3 ± 3.1 days	-	-
time from infection to admission	6.3 ± 3.7 days	3.6 ± 2.1 days	6.9 ± 2.7 days
pathogen-independent parameters			
maximum generation interval		$m_g = 15$ days	
maximum time from infection to reporting		$m_r = 25$ days	
maximum time from infection to admission		$m_h = 25$ days	
Gaussian process signal s.d.		$s_0 = 0.1$	
Gaussian process autocorrelation time scale		$l = 30$ days	
Gaussian process observation noise s.d.		$s_n = 0.001$	
probability of infection being reported		$p_c = 1$	
dispersion parameter for observed daily cases		$k_c = 25$	
dispersion parameter for observed daily admissions		$k_h = 25$	
coefficient of variation of the initial case–hospitalization ratio		$P_{CV} = 0.025$	

where $F(y)$ is the cumulative distribution function for the forecast and $\mathbb{I}(.)$ denotes the indicator function. CRPS was calculated numerically using 2000 randomly selected particles. The CRPS was calculated on log-transformed values so that it can be interpreted as a measure of relative rather than absolute error in forecast counts [29].

The code used to produce the results in this article is publicly available [30].

3. Results

We begin by summarizing the overall epidemic trends of SARS-CoV-2, influenza and RSV as seen retrospectively in the full season's data (§3.1). Then we describe the real-time weekly reporting that we carried out throughout the season (§3.2) and evaluate the performance of trend estimates and forecasts made in real time against subsequently available data (§3.3,3.4).

3.1. Overall epidemic trends

SARS-CoV-2 cases began increasing in New Zealand from April 2025 (figure 1). Cases increased until late June/early July when a peak in modelled cases (i.e. the expected number of daily cases excluding day-of-the-week effects) was reached (approximately 28 cases per day). Cases decreased for approximately two weeks before stabilizing, following a small resurgence in the epidemic growth rate from mid-July. SARS-CoV-2 cases were then stable until mid-August, before declining until the end of the study period (October). SARS-CoV-2 hospitalizations exhibited broadly similar temporal dynamics to SARS-CoV-2 cases (figure 2). The rise in SARS-CoV-2 cases and hospitalizations coincided with an increase in the proportion of genomically sequenced cases that were due to the NB.1.8.1 lineage, which increased from

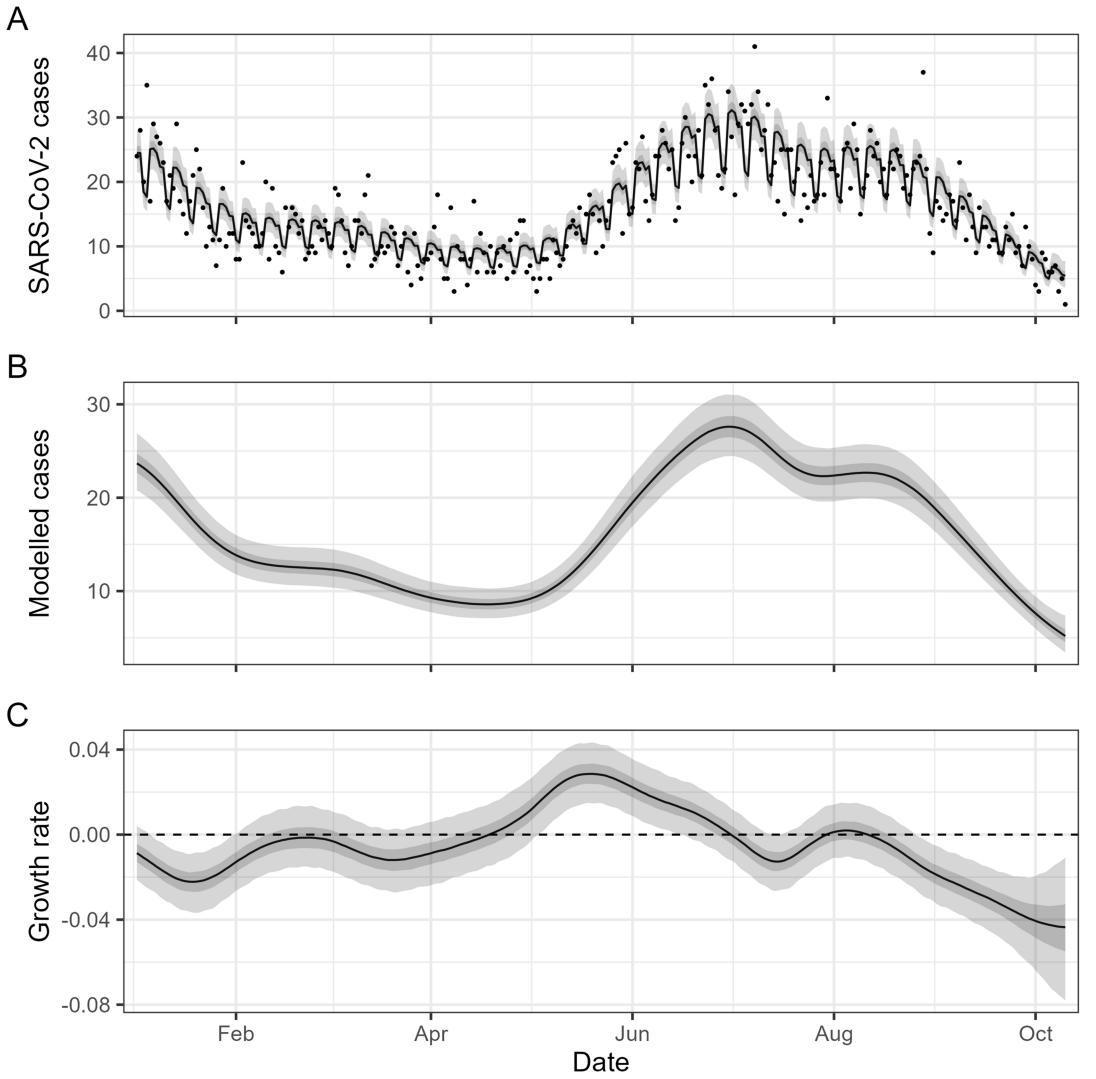

Figure 1. Modelled trends in SARS-CoV-2 cases fitted to full season data. (A) Daily SARS-CoV-2 cases (points) and modelled trends (i.e. the expected value of the time series) in SARS-CoV-2 cases using a Bayesian P-spline model, including a day-of-the-week effect (line and shaded region). (B) Modelled trend in SARS-CoV-2 cases (with day-of-the-week effect removed yet still included in the model). (C) Growth rate inferred from the modelled trend in SARS-CoV-2 cases (with day-of-the-week effect removed). The dashed line indicates a growth rate of zero, reflecting the threshold between epidemic growth or decline. For all panels, we include the model posterior distribution's median (line) and 50% and 95% credible intervals (dark shaded and light shaded regions).

low levels in early May to around 90% by the end of July [31]. This introduction of a new variant with a transmission advantage over established variants potentially contributed to overall growth in SARS-CoV-2 epidemic activity.

There were two peaks in influenza hospitalizations over the course of the season: one in late June; and one in mid-September. There was only one peak in RSV hospitalizations, occurring in early July. It is not clear when the modelled daily number of influenza and RSV hospitalizations began increasing (i.e. growth rate greater than 0) due to the low daily numbers of outcomes in these time series and the resulting high level of uncertainty estimated by the statistical smoothing model for the time when the growth rate became positive. Modelled trends in influenza and RSV hospitalizations were sensitive to the assumed prior distribution for the parameter controlling the smoothness of the second-order random walk, τ. When the mean of the prior distribution for τ was greater (i.e. less smooth), the model estimated sharper changes in the growth rate and wider credible intervals (see supplementary material, fig. S1).

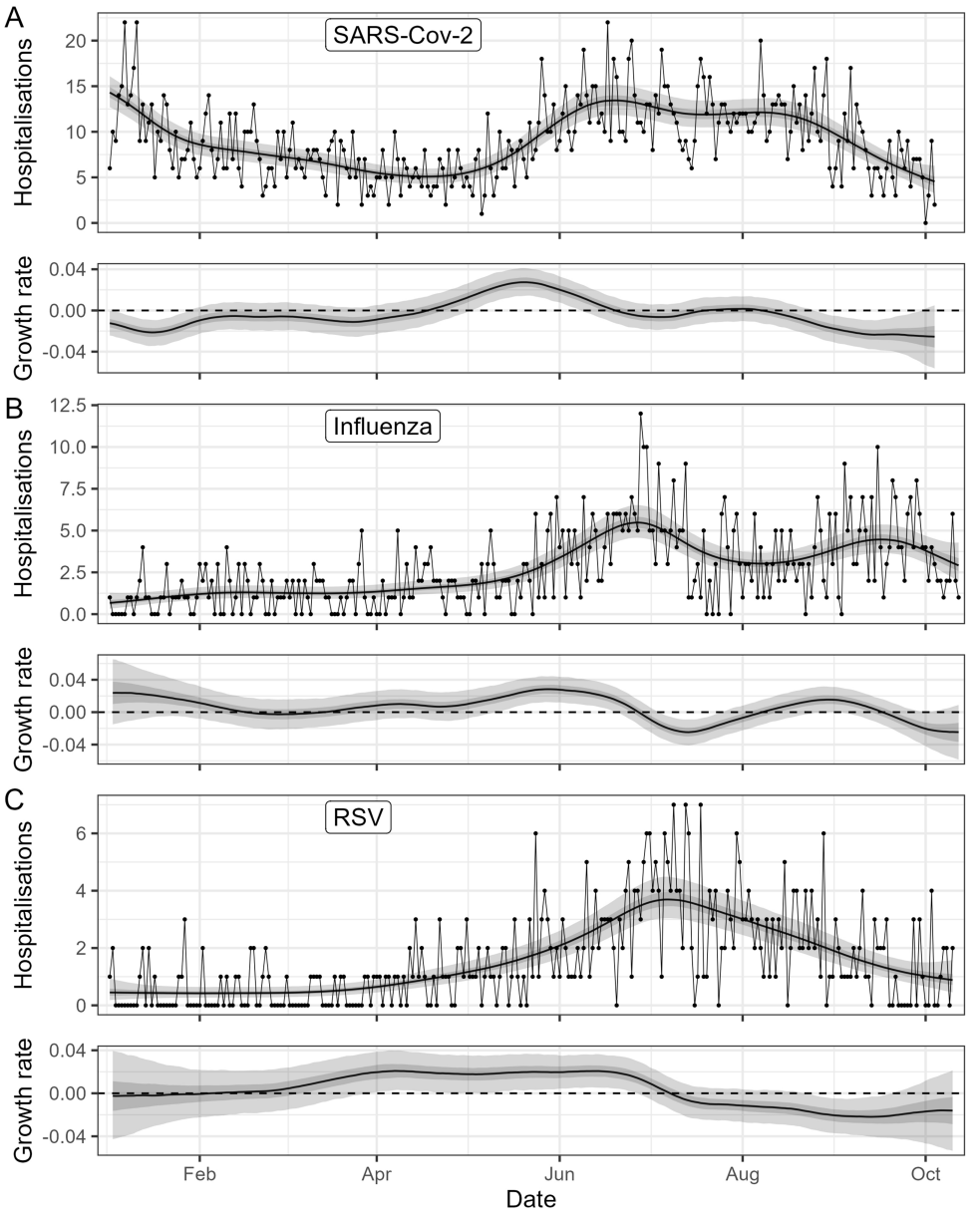

Figure 2. Modelled trends in hospitalizations fitted to full season data for: (A) SARS-CoV-2; (B) influenza; and (C) RSV. In the top panel for each pathogen, we plot the daily number of hospitalizations (points) and modelled trend (i.e. the expected value of the time series) in hospitalizations (line and shaded regions) using a Bayesian P-spline model that does not include a day-of-the-week effect. In the bottom panel for each pathogen, we plot the growth rate inferred from the modelled trend in hospitalizations. The dashed line indicates a growth rate of zero (the threshold between epidemic growth or decline). For all panels, we include the model posterior distribution's median (line) and 50% and 95% credible intervals (dark shaded and light shaded regions).

3.2. Real-time reporting

We analysed case and hospitalization time series in real time during the 2025 season, producing 15 reports for distribution to the New Zealand Ministry of Health and Te Whatu Ora Health New Zealand from 6 June (Report 1) to 3 October 2025 (Report 15). Each report presented estimates of past and current trends in cases and hospitalizations—including estimates of growth rates, doubling/halving times and the probability that the growth rate was greater than zero (cases/hospitalizations growing)—and, where available, 28-day ahead forecasts. An example report (Report 6, produced on 1 August 2025) is included in supplementary material, §S3. We chose Report 6 because earlier reports did not include forecasts as these were being developed and tested on previous season's data. Owing to reporting delays, the results

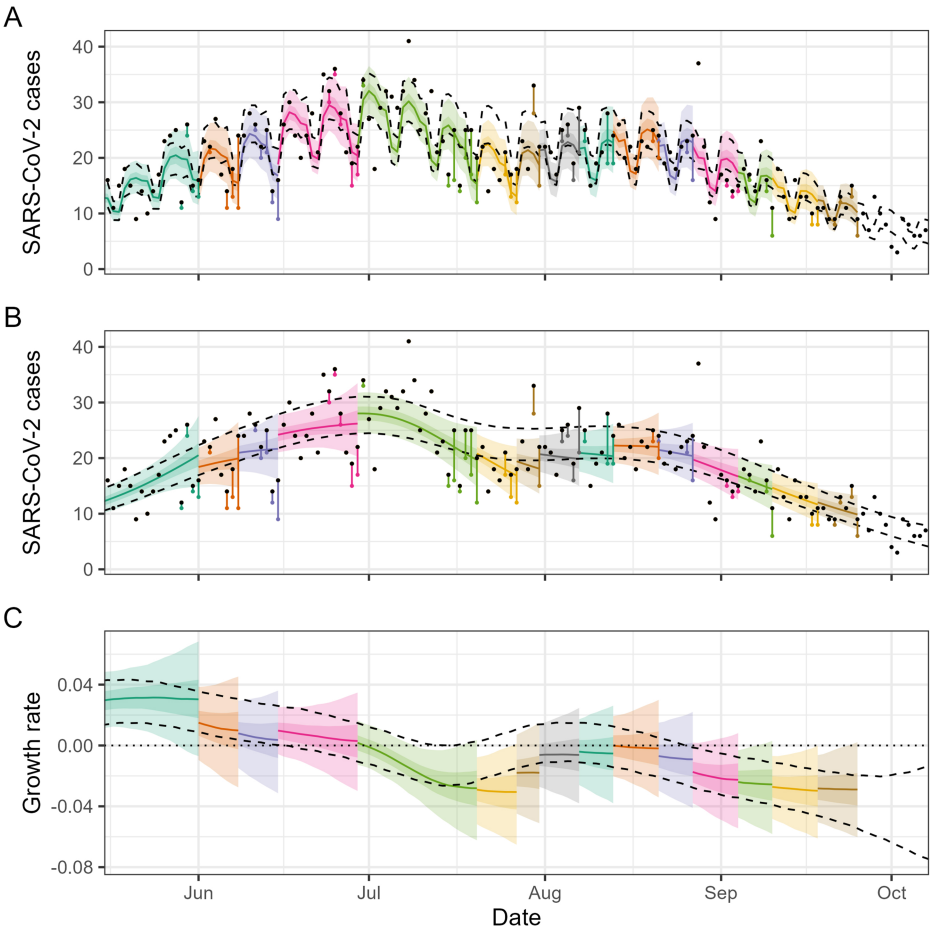

Figure 3. Modelled trends in SARS-CoV-2 cases reported in real time over the course of the season. (A) Modelled trends in SARS-CoV-2 cases including day-of-the-week effect (lines and shaded region). (B) Modelled trends in SARS-CoV-2 cases with day-of-the-week effect removed (lines and shaded region). (C) Growth rate (lines and shaded region) inferred from the modelled trend in SARS-CoV-2 cases (with day-of-the-week effect removed). For all panels, real-time estimates (coloured lines and shaded regions) are compared to 95% credible intervals of end-of-season estimates (black dashed lines). For all real-time estimates (coloured by round), we include the model posterior distribution's median (line) and 50% and 95% credible intervals (dark shaded and light shaded regions). We include the real-time model estimates up to the final day of data (for periods greater than the previous round's final day of data). In (A) and (B), the daily SARS-CoV-2 cases for the final end-of-season dataset (black points) and the daily SARS-CoV-2 cases in the real-time datasets (points coloured by round) are connected by lines to highlight revisions to data used in real-time analyses. For example, during the fourth round (first pink) there are visible pink data points connected directly to the black end-of-season data; the data in pink represent the data available when models were estimated and the data were revised upwards in the following round where they matched the end-of-season data. Note that when coloured points (and connecting lines) cannot be seen, then there have been no revisions to the data. When a coloured point can be seen and is the same colour as the real-time estimate for the same period (and connected directly to a black data point), it indicates that the number of cases for a specific day was revised (upwards in most instances) in the following round of data, but was not revised in any further rounds of data.

in this report were based on data up to 27 July 2025 for SARS-CoV-2 and 19 July 2025 for influenza and RSV. Forecasts show a 28-day time horizon from these respective origin dates.

3.3. Evaluation of real-time estimates of past and current trends

We compared estimates made in real time over the course of the season to final end-of-season estimates made with data available after season reporting had finished (final data received 23 October 2025). Real-time estimates of trends in SARS-CoV-2 cases showed good agreement with the end-of-season estimate, with overlapping 95% credible intervals (figure 3). The largest disagreements between real-time and end-of-season estimates were observed in late July (Reports 5–7), when real-time estimates suggested

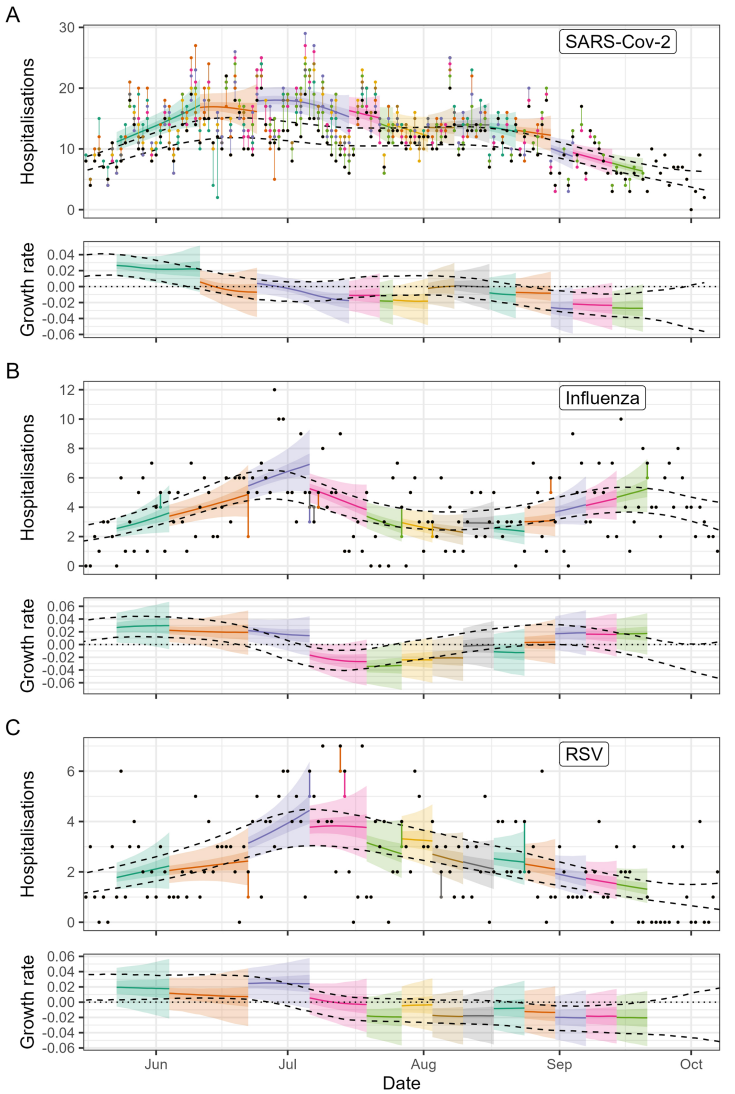

Figure 4. Modelled trends in hospitalizations reported in real time over the course of the season. Modelled trends in hospitalizations are shown for (A) SARS-CoV-2; (B) influenza; and (C) RSV. For each pathogen, we plot: (top panels) modelled trends in hospitalizations (lines and shaded region) and (bottom panels) growth rate (lines and shaded region) inferred from the modelled trend in hospitalizations. For all panels, real-time estimates (coloured lines and shaded regions) are compared to 95% credible intervals of end-of-season estimates (black dashed lines). For all real-time estimates (coloured by round), we include the model posterior distribution's median (line) and 50% and 95% credible intervals (dark shaded and light shaded regions). We include the real-time model estimates up to the final day of data (for periods greater than the previous round's final day of data). The daily number of hospitalizations for the final end-of-season dataset (black points) and the daily number of hospitalizations in the real-time datasets (points coloured by round) are connected by lines to highlight revisions to data used in real-time analyses. Note that when coloured points (and connecting lines) cannot be seen, then there have been no revisions to the data. Note that for SARS-CoV-2 hospitalizations some data were revised in multiple rounds, and so many points can be seen for the same time point.

epidemic activity was decreasing faster than estimated at the end of the season. During this period, there was a transient increase in the epidemic growth rate. There were also substantial revisions to the data received in real time (counts were revised upwards in the following week's data) (figure 3 and supplementary material, fig. S3), which biased our real-time estimates downwards (see supplementary material, fig. S2).

Real-time estimates of expected SARS-CoV-2 hospitalizations were higher than the end of season estimate for most rounds of reporting (figure 4). This was probably due to significant revisions to data (supplementary material, fig. S4) made over the entire study period (e.g. data available in the first round of reporting were revised multiple times over the study period). RSV and influenza hospitalization data

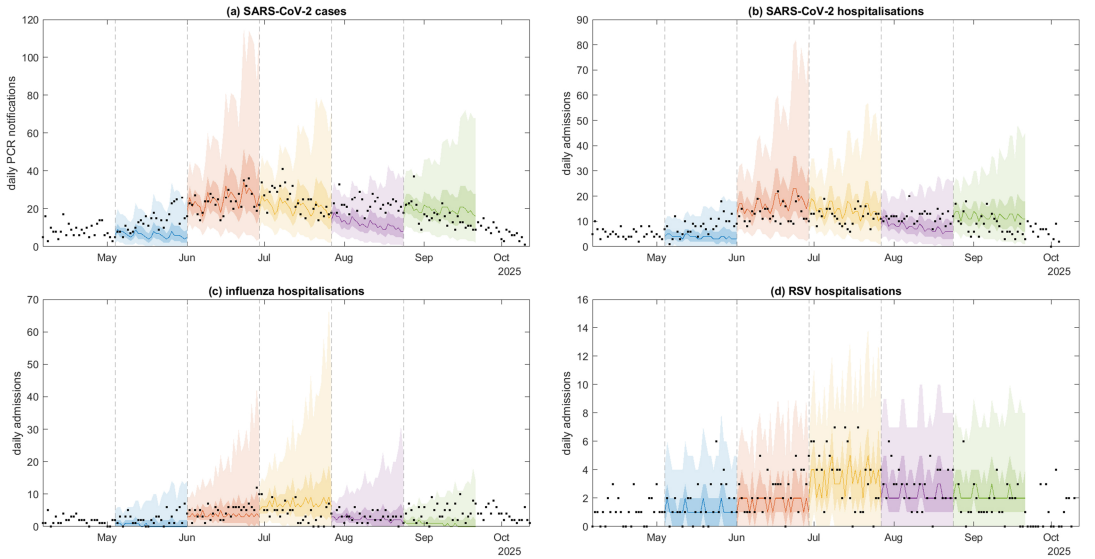

Figure 5. In-season 28-day ahead forecasts (coloured lines and bands) alongside subsequently observed data (black points) for (a) daily SARS-CoV-2 cases; (b) daily SARS-CoV-2 hospitalizations; (c) daily influenza hospitalizations; (d) daily RSV hospitalizations. Each coloured block shows a forecast generated at a specific origin date (shown by the vertical dashed lines), showing the posterior median (line) and 50% and 95% credible intervals (dark shaded and light shaded regions).

were far more stable, with fewer revisions made to the data (and data for a single date revised at most once). Accordingly, real-time estimates of expected hospitalizations and their trends for influenza and RSV showed greater agreement with end-of-season estimates (compared to SARS-CoV-2). The greatest disagreement was observed close to the peaks in hospitalizations, where real-time estimates suggested epidemic activity was continuing to increase. However, the lower credible intervals of these estimates were still captured within the end-of-season estimates.

3.4. Evaluation of real-time 28-day ahead forecasts

To evaluate forecast performance, we compared 28-day ahead forecasts produced for weekly origin dates (20 rounds from 4 May 2025 to 14 September 2025) against subsequently available data for the whole season (figure 5). For ease of visualization, figure 5 shows every fourth round so that the forecast periods do not overlap in time; supplementary material, figs. S6–S9 show forecasts for all rounds.

At the beginning of the season, SARS-CoV-2 forecasts were slow to pick up the increase in epidemic activity, and the early forecasts (e.g. blue blocks in figure 5a,b) underestimated subsequent data, although the data mostly fell within the 95% credible interval. For the remainder of the season, forecasts captured the data reasonably well, with the exception of a few rounds where the forecast systematically underestimated or overestimated the data (e.g. purple block in figure 5a). However, overall interval coverage properties were good, with 99.5% of data points for cases and 97.7% for hospitalizations falling within the 28-day ahead forecast 95% credible intervals (see supplementary material, table S1). An example set of model outputs for SARS-CoV-2 including latent variables, is shown in supplementary material, fig. S5. This shows that the model provided a good fit to training data and the estimated case–hospitalization ratio P_t varied little over the relevant time period.

Influenza forecasts (figure 5c) performed reasonably well, with good interval coverage throughout the season (99.6% of data fell within the 28-day ahead 95% credible intervals (see supplementary material, table S1)), although with wider credible intervals (compared to SARS-CoV-2). This is probably a consequence of the relatively small numbers of influenza hospitalizations in the data (recalling that influenza and RSV data were obtained from a regional sentinel surveillance programme, and so are not comparable with SARS-CoV-2 data). For the 29 June origin date (yellow block in figure 5c), which was around the peak in influenza activity, the forecast exhibited very wide credible intervals and somewhat overestimated subsequent data. The following week's forecast (yellow block in supplementary material, fig. S8b) provided a better prediction of the subsequent trend. Previous analyses have found that respiratory disease forecasts tend to perform worse and/or have high uncertainty near to the epidemic

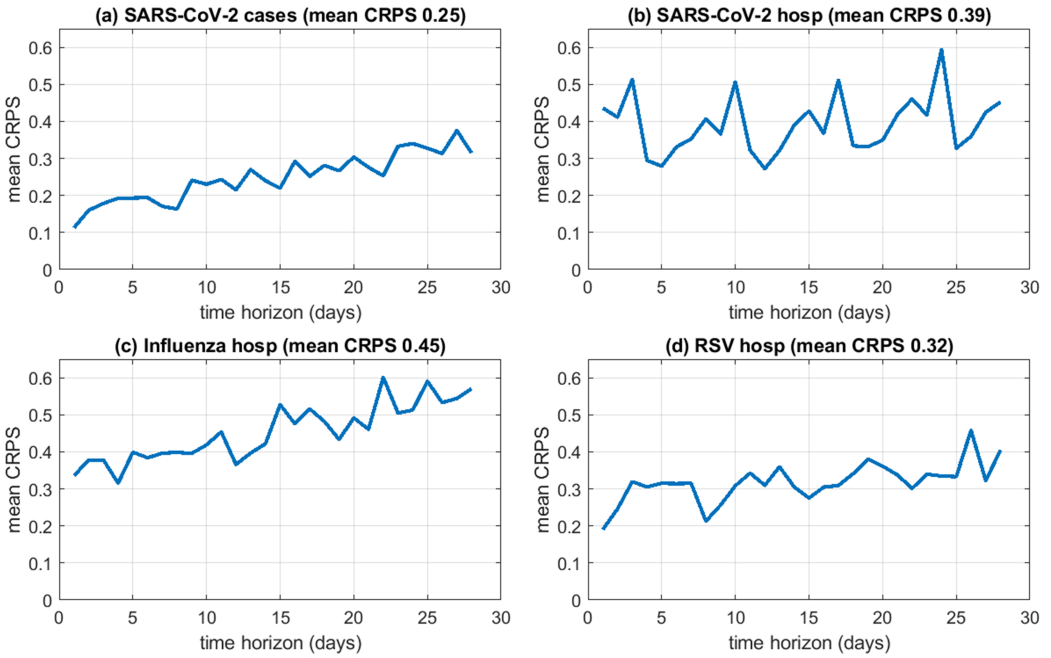

Figure 6. Mean CRPS at different forecast horizons for each of the forecast targets: (a) SARS-CoV-2 cases; (b) SARS-CoV-2 hospitalizations; (c) influenza hospitalizations; (d) RSV hospitalizations. CRPS values were calculated on log-transformed data and averaged over all rounds for a given forecast horizon. The value for mean CRPS shown in the text above each panel shows the CRPS averaged over all rounds and forecast horizons for that target.

peak [32]. However, although this was true of some of our forecasts, it was not universally true of all forecasts near the peak (see supplementary material, figs. S6–S9), potentially because these peaks were quite gradual with relatively modest rates of growth and decay and high levels of noise in the data.

RSV forecasts (figure 5d) also performed well at predicting the trend and displayed good interval coverage (98.2% of data fell within the 28-day ahead 95% credible intervals; see supplementary material, table S1). The 95% credible forecast intervals almost always included zero, reflecting the high frequency of zero counts throughout the relevant time period. RSV forecasts tended to be less sensitive to short-term fluctuations in the data compared to SARS-CoV-2 and influenza, probably due in part to its longer generation interval.

Figure 6 shows the mean CRPS for each forecast target as a function of the forecast time horizon, averaged over all rounds. The CRPS can be interpreted as a measure of the relative difference between the probabilistic forecast distribution and the subsequent data point; that is, a smaller CRPS indicates better forecast performance. For most forecast targets, there was an increasing trend of mean CRPS with time horizon, indicating that as expected, forecasts tended to perform worse as the time horizon increased. Overall, the forecasts for SARS-CoV-2 cases (figure 6a) had the best CRPS (mean 0.25). The forecast for SARS-CoV-2 hospitalizations (figure 6b) had a higher CRPS (mean 0.39) and showed signs of weekly periodicity with spikes at time horizons of 3, 10, 17 and 24 days. This could be due to a day-of-the-week effect that was not fully captured by the model, or due to historical revision of data primarily occurring on the same day of the week. Influenza had the worst CRPS of the four targets (mean 0.45), while RSV was intermediate (mean 0.32). The fact that forecast coverage was somewhat higher than the nominal interval coverage at the 50% and 95% levels for all four targets (see supplementary material, table S1) suggests that the forecast model is overly conservative in its uncertainty quantification, which will contribute to poorer CRPS scores.

4. Discussion

We have presented the methods and results of a 2025 New Zealand winter situational assessment programme for SARS-CoV-2, influenza and RSV. This was the first year of the programme; prior to 2025, New Zealand lacked capacity for real-time model-based situational assessment and forecasting for seasonal

respiratory diseases. This programme complements traditional surveillance of respiratory disease [24] by improving our ability to interpret and predict epidemiological trends in real time.

Our forecasts and estimates of current trends performed reasonably well overall, but were worse during periods of rapid change in the epidemic growth rate. This was not a surprising finding. Both models used in our analyses are fundamentally designed to estimate the current trend in the data; the forecast model assumes that this trend continues into the near future, with some gradual reversion to a prior distribution for the effective reproduction number over time. As a consequence, our models cannot predict trends before they start to become apparent in the data. While the two models had different objectives and are not directly comparable, they were often in broad agreement on the direction of epidemic trends (i.e. growing or declining). Small disagreements were observed between the models for SARS-CoV-2 cases in early June; central estimates of the growth rate were greater than zero, but central estimates of the forecasts predicted decreases in cases. However, the uncertainty in both model estimates led to substantially overlapping credible intervals, resulting in a relatively consistent epidemiological picture or assessment.

Estimates of current trends in SARS-CoV-2, influenza and RSV made by the trend analysis model during 2025 will have been influenced by trends in SARS-CoV-2 data from previous seasons. The model used for trend analysis penalizes changes in the epidemic growth rate, with the degree of penalization set by a parameter (τ). As such, estimates of current trends are sensitive to the value of τ. The models fit to SARS-CoV-2 cases, and hospitalizations estimated τ from the previous three years of SARS-CoV-2 data and, therefore, estimates will have been influenced by the epidemic dynamics (or the degree to which the growth rate varies over time) over this time period. For influenza and RSV hospitalizations, we only had access to less than one year of data, and therefore assumed an informative prior for τ (and the overdispersion in the negative binomial distribution) to achieve model convergence. These informative prior distributions were based on posterior distributions from the model fit to SARS-CoV-2 hospitalizations, which may not be indicative of the expected dynamics for influenza and RSV. In future years, as more data for influenza and RSV hospitalizations become available, we will aim to estimate all parameters for each pathogen individually.

Our models are likely to be biased when substantial revisions occur to data received in real time relative to the final data. SARS-CoV-2 cases recorded in the most recent week of data were regularly revised upwards in the following round of data (and influenza and RSV hospitalizations to a lesser extent). This probably biased estimates of current trends and forecasts downwards, but estimates of past trends would have been less affected. By contrast, SARS-CoV-2 hospitalizations were revised frequently, with the same day of data often revised over multiple rounds, biasing estimates of past, current and future trends. Statistical methods could be developed to quantify revisions in hospitalization or case counts over time. Existing methods rely on having sufficient data about when and how many counts are revised (i.e. two date variables, one for the date of occurrence and one for the date of receipt). Our methods could correct for the expected degree of revision in future seasons based on the 15 rounds of data received in 2025. For example, this could be done by fitting a model for the probability $P(n, m, s)$ that the final count for a given date t is n given that the observed count is m, according to data available at time $t + s$. This would enable these changes and associated uncertainty to be accounted for when estimating epidemic trends in real time, as has been done elsewhere [33]. However, we did not have sufficient information to perform such an analysis in advance of the 2025 season because we only had access to a single dataset for previous seasons, with no information on how those data would have been received and revised in real time.

The timing of peaks in epidemic activity of respiratory pathogens may be affected by school holidays, which have been estimated to reduce transmission of seasonal respiratory diseases [34]. School holidays in New Zealand ran from 28 June to 13 July 2025, and peaks in SARS-CoV-2 cases and influenza and RSV hospitalizations occurred around this period. School holidays can affect both transmission (by altering contact patterns) as well as testing and healthcare-seeking behaviour, which will influence case and hospitalization time series. Without more detailed data on behaviour [35] or underlying infection levels (as opposed to cases) [36], we cannot disentangle the underlying reasons for these changes. It is also possible that similarly timed peaks would have occurred irrespective of school holidays due to depletion of the susceptible population.

In 2025, an extended influenza season was experienced in southern hemisphere countries, including New Zealand, driven by the emergence of the antigenically distinct subclade K of influenza A/H3N2. Genomic data indicate that this virus was probably seeded into New Zealand from Australia in August 2025 [37] and caused influenza activity to continue into November and December at unusually high levels for the time of year. At the same time, northern hemisphere countries experienced unusually early

influenza activity as a result of the same variant [38,39]. Our results showed an increase in influenza activity in the last few weeks of our analysis (early September). However, most of the subclade K-driven influenza activity in New Zealand occurred after our regular analysis and reporting had ended for the season.

In future seasons, we aim to build on the platform established by this work. Objectives for future work include expanding the hub approach to include more forecasting models and reporting an ensemble forecast; developing statistical methods to account for revisions to data received in real time; expanding the types of analysis reported, for example to include the size and timing of the epidemic peak as explicit forecast targets; and incorporating national data on influenza hospitalizations from the National Minimum Dataset [40]. The ACEFA forecasting hub also runs a winter situational assessment programme for Australian states and territories, providing weekly reports comparable to those described here for New Zealand (e.g. [41,42]). We are working towards producing a combined trans-Tasman weekly report covering both countries, subject to data sharing and confidentiality agreements. This would enable the timely exchange of surveillance intelligence between Australia and New Zealand and build joint capability in real-time epidemic analytics for public health partners.

Ethics. This work did not require ethical approval from a human subject or animal welfare committee.

Data accessibility. Data and relevant code for this research work are stored in GitHub: http://github.com/michaelplanknz/ACEFA-NZ-winter-SAP-2025 and have been archived within the Zenodo repository [43].

Supplementary material is available online [44].

Declaration of AI use. We have not used AI-assisted technologies in creating this article.

Authors' contributions. M.J.P.: conceptualization, investigation, methodology, software, visualization, writing—original draft, writing—review and editing; A.R.Y.: data curation, software, validation, writing—review and editing; K.L.S.: data curation, software, validation, writing—review and editing; R.T.: data curation, software, validation, writing—review and editing; M.O'H.-W.: software, validation, visualization, writing—review and editing; F.C.: conceptualization, data curation, writing—review and editing; F.M.S.: conceptualization, funding acquisition, methodology, project administration, supervision, writing—original draft, writing—review and editing; O.E.: conceptualization, investigation, methodology, software, visualization, writing—original draft, writing—review and editing.

All authors gave final approval for publication and agreed to be held accountable for the work performed therein.

Conflict of interest declaration. We declare we have no competing interests.

Funding. M.J.P. was supported by a grant from the Marsden Fund (24-UOC-020) and from Te Niwha Infectious Diseases Research Platform, co-hosted by PHF Science and the University of Otago and provisioned by the Ministry of Business, Innovation and Employment, New Zealand (TN/P/24/UoC/MP). O.E. was supported by a University of Melbourne McKenzie fellowship. F.M.S. was supported by the National Health and Medical Research Council of Australia through the Investigator Grant Scheme (Emerging Leader Fellowship, 2021/GNT2010051). This research is supported by the Australia–Aotearoa Consortium of Epidemic Forecasting and Analytics (ACEFA), a National Health and Medical Research Council of Australia Centre of Research Excellence (2 035 303).

Acknowledgements. We are grateful to Te Whatu Ora (Health New Zealand), Manatū Ora (Ministry of Health) and Public Heath and Forensic Science for providing weekly data updates throughout the 2025 winter respiratory season and feedback on the content of the weekly reports, in particular Andy Anglemeyer, Harriette Carr, Laura Cleary, Susan Jack, Bex Joslin, Tomasz Kiedrzynski, Zoe Kumbaroff, Andrea McNeill, Natasha Rafter, Imogen Roth, Tanisha Selvaratnam and Fiona Wild. The authors are grateful to Rob Hyndman for feedback on the forecasting model methodology and to Alex Kazemi and three anonymous reviewers for comments on an earlier version of this manuscript.

References

1. Moss R, Fielding JE, Franklin LJ, Stephens N, McVernon J, Dawson P, McCaw JM. 2018 Epidemic forecasts as a tool for public health: interpretation and (re) calibration. *Aust. N. Z. J. Public Health.* **42**, 69–76. (doi:10.1111/1753-6405.12750)
2. Lutz CS *et al*. 2019 Applying infectious disease forecasting to public health: a path forward using influenza forecasting examples. *BMC Public Health.* **19**, 1659. (doi:10.1186/s12889-019-7966-8)
3. Gozzi N *et al*. 2025 Performance evaluation of RespiCast ensemble forecasts for primary care syndromic indicators of viral respiratory disease in Europe during the 2023/24 winter season. *medRxiv.* (doi:10.1101/2025.10.30.25339155)
4. Eales O, McCaw JM, Shearer FM. 2024 Biases in routine influenza surveillance indicators used to monitor infection incidence and recommendations for improvement. *Influenza Other Respi. Viruses* **18**, e70050.
5. Eales O, Windecker SM, McCaw JM, Shearer FM. 2025 Inferring temporal trends of multiple pathogens, variants, subtypes or serotypes from routine surveillance data. *Am. J. Epidemiol.* **194**, 2489–2498. (doi:10.1093/aje/kwaf119)

6. Yang W, Cowling BJ, Lau EH, Shaman J. 2015 Forecasting influenza epidemics in Hong Kong. *PLoS Comput. Biol.* **11**, e1004383. (doi:10.1371/journal.pcbi.1004383)
7. Zarebski AE, Dawson P, McCaw JM, Moss R. 2017 Model selection for seasonal influenza forecasting. *Infect. Dis. Model.* **2**, 56–70. (doi:10.1016/j.idm.2016.12.004)
8. Reich NG *et al*. 2016 Challenges in real-time prediction of infectious disease: a case study of dengue in Thailand. *PLoS Negl. Trop. Dis.* **10**, e0004761. (doi:10.1371/journal.pntd.0004761)
9. Chowell G *et al.* 2016 Using phenomenological models to characterize transmissibility and forecast patterns and final burden of Zika epidemics. *PLoS Curr. Outbreaks* **8**. (doi:10.1371/currents.outbreaks.f14b2217c902f453d9320a43a35b9583)
10. Funk S, Camacho A, Kucharski AJ, Lowe R, Eggo RM, Edmunds WJ. 2019 Assessing the performance of real-time epidemic forecasts: a case study of Ebola in the Western Area region of Sierra Leone, 2014-15. *PLoS Comput. Biol.* **15**, e1006785. (doi:10.1371/journal.pcbi.1006785)
11. Finger F, Funk S, White K, Siddiqui MR, Edmunds WJ, Kucharski AJ. 2019 Real-time analysis of the diphtheria outbreak in forcibly displaced Myanmar nationals in Bangladesh. *BMC Med.* **17**, 58. (doi:10.7490/f1000research.1115484.1)
12. Cramer EY *et al*. 2022 Evaluation of individual and ensemble probabilistic forecasts of COVID-19 mortality in the United States. *Proc. Natl Acad. Sci.* **119**, e2113561119. (doi:10.1073/pnas.2113561119)
13. Moss R, Price DJ, Golding N, Dawson P, McVernon J, Hyndman RJ, Shearer FM, McCaw JM. 2023 Forecasting COVID-19 activity in Australia to support pandemic response: May to October 2020. *Sci. Rep.* **13**, 8763. (doi:10.1101/2022.08.04.22278391)
14. Sherratt K *et al*. 2023 Predictive performance of multi-model ensemble forecasts of COVID-19 across European nations. *eLife* **12**, e81916. (doi:10.7554/eLife.81916)
15. Plank MJ, Watson L, Maclaren OJ. 2024 Near-term forecasting of Covid-19 cases and hospitalisations in Aotearoa New Zealand. *PLoS Comput. Biol.* **20**, e1011752. (doi:10.1371/journal.pcbi.1011752)
16. ACEFA. 2026 Australia-Aotearoa Consortium for Epidemic Forecasting and Analytics. Available from https://acefa-epi-analytics.org/.
17. Wood SN. 2017 P-splines with derivative based penalties and tensor product smoothing of unevenly distributed data. *Stat. Comput.* **27**, 985–989. (doi:10.1007/s11222-016-9666-x)
18. Fraser C. 2007 Estimating individual and household reproduction numbers in an emerging epidemic. *PLoS ONE* **2**, e758. (doi:10.1371/journal.pone.0000758)
19. Abbott S *et al*. 2020 Estimating the time-varying reproduction number of SARS-CoV-2 using national and subnational case counts. *Wellcome Open Res.* **5**, 112. (doi:10.12688/wellcomeopenres.16006.1)
20. Steyn N, Parag KV, Thompson RN, Donnelly CA. 2025 A primer on inference and prediction with epidemic renewal models and sequential Monte Carlo. *Stat. Med.* **44**, e70204. (doi:10.1002/sim.70204)
21. Statistics NZ. 2025 Subnational population estimates: at 30 June 2025; Available from https://www.stats.govt.nz/information-releases/subnational-population-estimates-at-30-june-2025/.
22. Te Whatu Ora Health New Zealand. 2025 National Minimum Dataset - hospital events. Available from https://www.healthnz.govt.nz/about-us/health-data/data-sets-and-collections/national-collections/national-minimum-dataset-hospital-events.
23. Huang QS *et al*. 2014 Implementing hospital-based surveillance for severe acute respiratory infections caused by influenza and other respiratory pathogens in New Zealand. *Western Pac. Surveill. Response J.* **5**, 23–30. (doi:10.5365/wpsar.2014.5.1.004)
24. Public Health and Forensic Science (previously ESR). 2025 2024 acute respiratory illness surveillance report. Available from: https://www.phfscience.nz/media/gj3bkkvp/2024acuterespiratoryillnesssurveillancereport.pdf.
25. Eales O *et al*. 2022 Appropriately smoothing prevalence data to inform estimates of growth rate and reproduction number. *Epidemics* **40**, 100604. (doi:10.1016/j.epidem.2022.100604)
26. Hoffman MD, Gelman A. 2014 The no-U-turn sampler: adaptively setting path lengths in Hamiltonian Monte Carlo. *J. Mach. Learn Res.* **15**, 1593–623.
27. Stan Development Team. RStan: the R interface to Stan. Available from https://mc-stan.org/.
28. Rasmussen CE, Williams CKI. 2006 *Gaussian processes for machine learning*. Cambridge, MA: MIT Press.
29. Bosse NI, Abbott S, Cori A, Van Leeuwen E, Bracher J, Funk S. 2023 Scoring epidemiological forecasts on transformed scales. *PLoS Comput. Biol.* **19**, e1011393. (doi:10.1101/2023.01.23.23284722)
30. Plank MJ, Eales O. 2026 GitHub repository: ACEFA-NZ-winter-SAP-2025. Available from https://github.com/michaelplanknz/ACEFA-NZ-winter-SAP-2025.
31. Public Health and Forensic Science. 2025 Covid-19 Genomics Insight Dashboard Report 62. Available from https://www.phfscience.nz/media/i4tle1xb/phf-science-cgid-report-62.pdf.
32. Lopez VK *et al*. 2024 Challenges of COVID-19 case forecasting in the US, 2020–2021. *PLoS Comput. Biol.* **20**, e1011200. (doi:10.1371/journal.pcbi.1011200)
33. Johnson KE *et al*. 2025 Baseline nowcasting methods for handling delays in epidemiological data. *Wellcome Open Res.* **10**, 614. (doi:10.12688/wellcomeopenres.25027.2)

34. Jackson C, Vynnycky E, Mangtani P. 2016 The relationship between school holidays and transmission of influenza in England and Wales. *Am. J. Epidemiol.* **184**, 644–51. (doi:10.1093/aje/kww083)
35. Eales O *et al*. 2025 Temporal trends in test-seeking behaviour during the COVID-19 pandemic. *Math. Med. Life Sci.* **2**, 2521858. (doi:10.1080/29937574.2025.2521858)
36. Eales O, McCaw JM, Shearer FM. 2024 Challenges in the case-based surveillance of infectious diseases. *R. Soc. Open. Sci.* **11**, 240202. (doi:10.1098/rsos.240202)
37. Dapat C *et al*. 2026 Extended influenza seasons in Australia and New Zealand in 2025 due to the emergence of influenza A(H3N2) subclade K viruses. *Eurosurveillance* **30**, 2500894. (doi:10.2807/1560-7917.es.2025.30.49.2500894)
38. Hay JA *et al.* 2025 Evaluation of the epidemiological outlook of the influenza A/H3N2 clade K in England during the 2025-26 season. *Zenodo pre-print* (doi:10.5281/zenodo.17704679)
39. Fieldhouse R. 2025 Japan declares a flu epidemic—what this means for other nations. *Nature*. (doi:10.1038/d41586-025-03367-z)
40. Te Whatu Ora Health New Zealand. 2025 National Minimum Dataset (hospital events). Available from https://www.tewhatuora.govt.nz/for-health-professionals/data-and-statistics/nz-health-statistics/national-collections-and-surveys/collections/national-minimum-dataset-hospital-events.
41. Eales O *et al.* 2026 Temporal analysis of respiratory virus epidemics in Victoria over winter 2024. *Commun. Dis. Intell.* **50**. (doi:10.33321/cdi.2026.50.015)
42. Henderson AS *et al*. 2026 Winter forecasting of respiratory viruses in Victoria Australia. *medRxiv*, 1–22. (doi:10.64898/2026.05.18.26353544)
43. Plank M, Eales O. 2026 michaelplanknz/ACEFA-NZ-winter-SAP-2025: Final published version (Version v1.1) [Computer software]. Zenodo. (doi:10.5281/zenodo.20868347)
44. Plank MJ, Young AR, Senior KL, Tobin R, O'Hara-Wild M, Callaghan F, Shearer FM, Eales O. 2026 Supplementary material from: Multi-pathogen situational assessment and forecasting of respiratory disease in Aotearoa New Zealand. Figshare. (doi:10.6084/m9.figshare.c.8598184)